EPR studies of interstitial Ni centers in synthetic diamond crystals

J. Isoya

University of Library and Information Science, Kasuga 1-2, Tsukuba-city, Ibaraki-ken, 305 Japan

H. Kanda and Y. Uchida

National Institute for Research in Inorganic Materials, Namiki 1-1, Tsukuba-city, Ibaraki-ken, 305 Japan

Two new electron-paramagnetic-resonance (EPR) spectra, tentatively labeled NIRIM-1 and NIRIM-2, have been studied using synthetic diamond crystals grown from the Ni solvent to which various amounts of nitrogen getters (Ti, Zr) and/or boron were added. The NIRIM-1 spectrum ($g = 2.0112$) having the effective spin $S = \frac{1}{2}$, which has been determined from the microwave pulse-width dependence of the two-pulse echo intensity, is assigned to be isolated interstitial Ni^+ with electronic configuration $3d^9$. The anisotropic spectra of powderlike line shape at 4 K might be ascribed to an intermediate Jahn-Teller effect coupled predominantly with trigonal distortions. The NIRIM-2 spectrum having an axially symmetric g tensor ($S = \frac{1}{2}$, $g_\parallel = 2.3285$, $g_\perp \approx 0$) arises from a $3d^9$ ion in a crystal field of trigonally distorted octahedron. It is proposed that the center is interstitial Ni^+ associated with a vacancy or with local charge compensation.

I. INTRODUCTION

Recent developments in the high-pressure synthesis of relatively large diamond crystals by the temperature-gradient method have opened up new applications of this material, utilizing its unique physical properties. Impurities and point defects, which usually spoil the unique physical properties, might sometimes create optical or electrical properties useful in practical applications.

Transition-metal ions of the $3d$ group diffuse easily into silicon at a temperature near the melting point, and deep levels are introduced. Synthetic diamond crystals are grown from a metal solvent such as Fe, Co, Ni, Mn or a combination of them. Thus, the growth conditions seem to be most favorable in incorporating transition-metal impurities into the lattice of diamond crystal. So far, nickel seems to be the only transition-metal ion that gives a well-established EPR signal ($g = 2.0319$) from dispersed impurities.[1-3] The site of the Ni center has been determined based on both the angular dependence of ^{13}C superhyperfine lines from the nearest-neighbor carbons measured by continuous-wave (cw) EPR and the angular dependence of ^{13}C electron-nuclear double resonance (ENDOR) lines from the next-nearest-neighbor carbons measured by electron-spin-echo envelope modulation (ESEEM) method.[3] With the effective spin $S = \frac{3}{2}$, which was measured by the transient nutation method, under the tetrahedral field of the substitutional site, the Ni center has been assigned to be Ni^- with electronic configuration $3d^7$.[3] The substitutional Ni^- center is, hereafter, designated as Ni_s^-.

Several absorption bands, being specifically observed in synthetic diamond crystals grown in the presence of nickel, have been ascribed to being associated with the incorporation of nickel. They are three vibronic bands with zero phonon lines of 1.40, 1.883, and 2.51 eV, respectively, a broad absorption between 0.8 and 2.0 eV with a maximum around 1.4 eV, and a sharp infrared absorption line at 1332 cm^{-1}.[4-6] Relative intensities of these absorption bands as well as the color of the crystals depend on the composition of the metal solvent when Ni-based alloys are used as the solvents. Some of the absorption bands above might be arising from positively (negatively) charged defect species, while not containing nickel atom(s), that are needed to keep the charge neutrality of the lattice with the presence of negatively (positively) charged nickel centers. The 1.40-eV system has been identified as being associated with the center containing one nickel atom from the fine structure caused by the different isotopes of nickel.[7] Crystals grown from a pure Ni solvent show neither a 1.40-eV absorption system nor a broad 1.4-eV band, while strong EPR signals of Ni_s^- are observed. It is likely that nickel can be incorporated not only as Ni_s^- but also in a form other than Ni_s^-.

In the present work, we have found two new EPR centers, which are assigned to be related to interstitial Ni^+ with electronic configuration $3d^9$.

II. EXPERIMENT

Synthetic diamond crystals were grown by the temperature-gradient method[8,9] using Ni solvents with various amounts of additives (Zr, Ti, and B). The metal solvents Ni, Ni-Zr, and Ni-Ti were formed into a disk 7 mm in diameter and 3 mm thick. As the carbon source, graphite powders (~ 80 mg) or a graphite disk 7 mm in diameter and 2 mm thick (~ 120 mg) was used. Seed crystals were placed below the metal disk separated from it by a platinum foil that prevented the seeds from dissolving into the metal solvent before crystals could grow.[10] An assembly of the carbon source and the metal

solvent with seed(s) was placed in a capsule made of NaCl–10 wt. % ZrO_2 powder compact. For boron doping, the desired amount of boron was added between the carbon source and the metal solvent. The pressure and the temperature of the growth were ~6 GPa and ~1700 K. Crystals (from one to three depending on the number of seeds used) with a diameter from 2 to to 3 mm were obtained in 15–24 h.

The continuous wave (cw) EPR spectra were taken using a Bruker ESP300 x-band spectrometer. The pulsed EPR measurements were made using a home-built spectrometer equipped with a 1-kW traveling-wave tube amplifier (TWTA) and a pulse programmer that controlled the pulse separation(s) with the minimum step of 5 ns. The pulse widths could be varied with the minimum step of 200 ps. The EPR measurements at 77 K were carried out by using an insertion Dewar filled with liquid nitrogen, and other temperatures were reached using an Oxford Instruments ESR-900.

III. RESULTS

A. NIRIM-1 center

1. Growth condition dependence

Typical synthetic diamond crystals, which exhibit a distinct yellow color, contain a substantial amount (50–300 ppm) of neutral nitrogen atoms in an isolated substitutional form. Yellow-colored crystals grown from Ni-based metal solvents show EPR signals of Ni_s^- in addition to those of neutral nitrogen atoms [Figs. 1(a) and 2(a)]. In the crystals grown from the Ni solvent without additives, the concentration of neutral nitrogen atoms was ~300 ppm. With the addition of a small amount of Zr or Ti to the Ni solvent, the concentration of neutral nitrogen atoms in the crystal is decreased. Zr and Ti, which are known as efficient getters of nitrogen atoms[11] prevent nitrogen from being incorporated into the crystal lattice, presumably by holding nitrogen atoms in the solution with strong affinity to them. By increasing the amount of the nitrogen getters added to the Ni solvents, crystals with green and/or brown colors were obtained. In these crystals, both the concentration of neutral nitrogen atoms and that of Ni_s^- are small and a new EPR signal (denoted here as NIRIM-1) (Ref. 12) appears at $g=2.0112$ [Figs. 1(b) and 2(b)]. By boron doping, p-type semiconducting crystals with a blue color are synthesized.[13] The concentration of neutral nitrogen atoms in the crystal is decreased by boron doping. A relatively strong signal of the NIRIM-1 center was observed for boron-doped crystals grown from Ni solvent with the addition of Ti [Figs. 1(c) and 2(c)]. The concentrations of neutral nitrogen atoms [N], that of Ni_s^- [Ni_s^-], and that of the NIRIM-1 center [NIRIM-1] measured from the EPR signal intensities for several typical crystals are listed in Table I. Since our crystals show nonuniform color distribution, the distribution of impurities in a crystal is likely to be nonuniform. From the EPR signal intensities and the weight of the crystals, the average concentration of each paramagnetic impurity for each crystal was es-
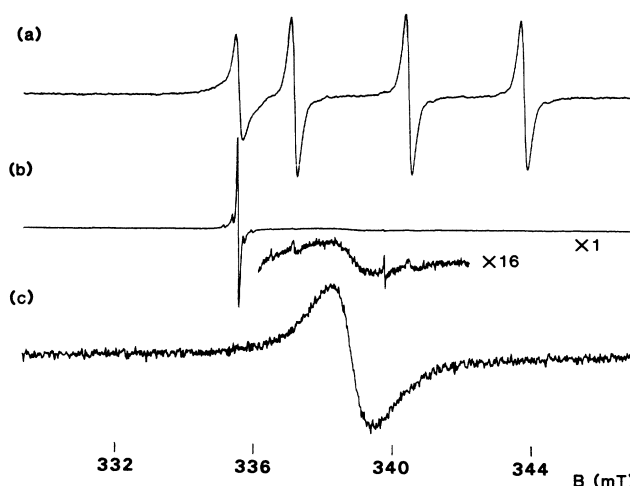

FIG. 1. cw EPR spectra of synthetic diamond crystals at 77 K with the magnetic field parallel to [001] ($\nu=9.5485$ GHz, 100 kHz field modulation). (a) Sample A (2 μW microwave power, 16 μT modulation amplitude) showing signals of Ni_s^- ($g=2.0319$) and isolated neutral nitrogens. (b) Sample F (0.2 mW, 10 μT) showing signals of Ni_s^- and the NIRIM-1 spectrum. (c) Sample M (0.2 mW, 10 μT) showing the NIRIM-1 spectrum.

timated. A slight variation in the impurity concentration was noticed among the crystals grown from different runs with the composition of the metal solvent fixed. The temperature of the growth varied from one sample to another, probably within the limits of ~100 K. Strict control and accurate measurement of the growth temperature has not been established yet in our laboratory. Thus, Table I shows the tendency of the impurities to be controlled by modifying the Ni solvent with the addition of nitrogen getters and/or by boron doping. The NIRIM-1 signal was not observed for crystals grown from the metal solvent not containing Ni. The NIRIM-1 signal was ob-
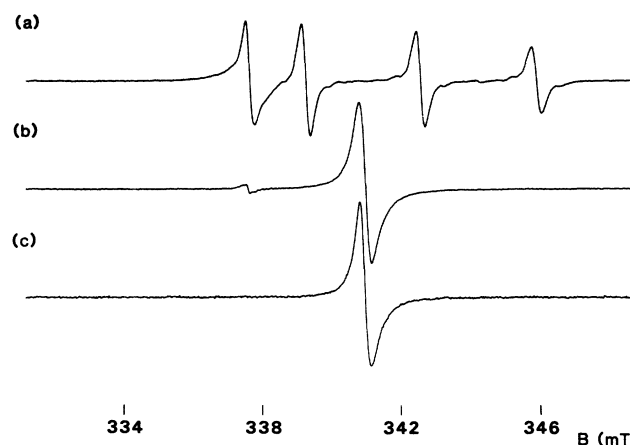

FIG. 2. cw EPR spectra of synthetic diamond crystals at ~25 K with the magnetic field parallel to [001] ($\nu=9.6009$ GHz, 100 kHz field modulation). (a) Sample A (0.5 μW microwave power, 50 μT modulation amplitude). (b) Sample F (0.5 mW, 20 μT). (c) Sample M (0.5 μW, 50 μT). A strong NIRIM-1 spectrum is observed for samples F and M.

TABLE I. Concentration of paramagnetic impurities in synthetic diamond crystals.

Sample	Composition of metal solvent	Amount of boron added (mg)	Color	Weight (mg)	[N]	[Ni_s^-]	[NIRIM-1]	Conductivity at 295 K ($\Omega^{-1}cm^{-1}$)
A	Ni–3.4 wt.% Zr		yellow	6.5	76	52		
B	Ni–3.5 wt.% Zr		yellowish green	7.3	21	68		
C	Ni-10 wt.% Zr		brown	6.4		0.01	1.5	
D	Ni-1 wt.% Ti		yellowish green	9.0	59	16		
E	Ni-2 wt.% Ti		green	9.2	1	0.4	0.07	
F	Ni-2 wt.% Ti		green/brown	13.1	2	0.3	4.2	
G	Ni-2 wt.% Ti		green/brown	19.7	3	3.8	6.1	
H	Ni	10	yellow	6.8	242	43		3×10^{-8}
I	Ni	10	yellow/blue	18.2	12	10		4×10^{-6}
J	Ni	20	yellow/blue	11.4	46		1.4	3.2×10^{-3}
K	Ni	20	blue	10.0			4.6	1.0×10^{-1}
L	Ni	40	blue	6.9				2.8
M	Ni-2 wt.% Ti	1	blue	16.0			7.5	1.2×10^{-4}
N	Ni-2 wt.% Ti	1	blue	5.1			3.6	1.0×10^{-4}
O	Ni-2 wt.% Ti	10	blue	9.9				5.4×10^{-1}

served both in nondoped crystals grown from the Ni solvent with Ti(Zr) added and in boron-doped crystals grown from the Ni solvent with or without adding Ti. Thus, the NIRIM-1 center is associated with the incorporation of Ni.

2. Temperature dependence

Between 25 and 77 K, the line position ($g=2.0112$) is independent of the orientation of the crystals with respect to the magnetic field, and the line shape is symmetric. In this temperature range, the linewidth increases as the temperature increases. At 4 K, the line shape is asymmetric and depends on the orientation of the crystal (Fig. 3). The line shape is similar to that of a powder sample with an anisotropic g tensor. The crystal (sample E) was rotated with the magnetic field in the ($\bar{1}10$) plane. With the rotation from the magnetic field parallel to the [001] axis (B‖[001]) to B‖[110], the separation between the low-field extreme and the high-field extreme increases from the minimum (0.66 mT) at B‖[001] to the maximum (1.30 mT) at B‖[111], then decreases (1.08 mT at B‖[110]). It is expected that paramagnetic species with trigonal symmetry should have four magnetically inequivalent sites in the diamond lattice. If these trigonal centers have a g tensor axially symmetric around one of the four threefold axes with the principal values $g_\parallel$ and $g_\perp$, a single line is observed at $g=g_{iso}=(g_\parallel^2/3+2g_\perp^2/3)^{1/2}$ for B‖[001]. For B‖[111], two lines with the intensity ratio 3:1 are observed at $g=(g_\parallel^2+8g_\perp^2)^{1/2}/3$ and at $g=g_\parallel$, respectively. For the rotation with the magnetic field in the ($\bar{1}10$) plane, the maximum splitting among the lines belonging to different sites occurs at B‖[111]. The angular dependence at 4 K indicates that the NIRIM-1 center undergoes a distortion, predominantly of trigonal symmetry. The powderlike line shape suggests either a distribution in the magnitude of trigonal

distortion or a significant contribution of random internal strains. The line shape becomes close to a conventional one at B‖[001], however, with a slight asymmetry (Fig. 3).

The temperature dependence of the line shape reveals that an isotropic line ($g=g_{iso}$) is superimposed on the anisotropic spectrum of a powder-pattern-like line shape (Fig. 3). As the temperature increases from 4 K, the isotropic line grows with the expense of the anisotropic spectra, while the separation between the extremes of the asymmetric powderlike spectra decreases. The motional narrowing occurs at a lower temperature when B is near the [001] direction than for B along [111]. A slight angular variation of the linewidth remains at ~25 K (ΔB_{pp} =0.35, 0.43, and 0.35 mT for B‖[001], B‖[111], and B‖[110], respectively, at 24 K for sample F). Above ~10 K, line broadening due to spin-lattice relaxation occurs parallel to the averaging process. The narrowest linewidth observed was ΔB_{pp} =0.20 mT for B‖[001] at 10 K.

The above angular dependence and the temperature dependence below 25 K were similarly observed for samples C, E, F, G, and M. The linewidth at 77 K, which did not vary upon rotation of the crystal, showed some sample dependence (ΔB_{pp} = 1.59, 1.35, and 1.17 mT for samples C, F, and M, respectively).

3. Effective spin

Under the cubic symmetry of either substitutional or interstitial sites, a single isotropic line is expected for all spin states with $S\le\frac{3}{2}$, since the fine-structure splittings vanish. The spin state can be determined from the fine structure observed for the distorted configurations at low temperatures. The absence of fine structure in the anisotropic spectrum at 4 K suggests that the spin state is $S=\frac{1}{2}$. Since the fine structure is often obscured by the line broadening due to random internal strains,[14] the spin
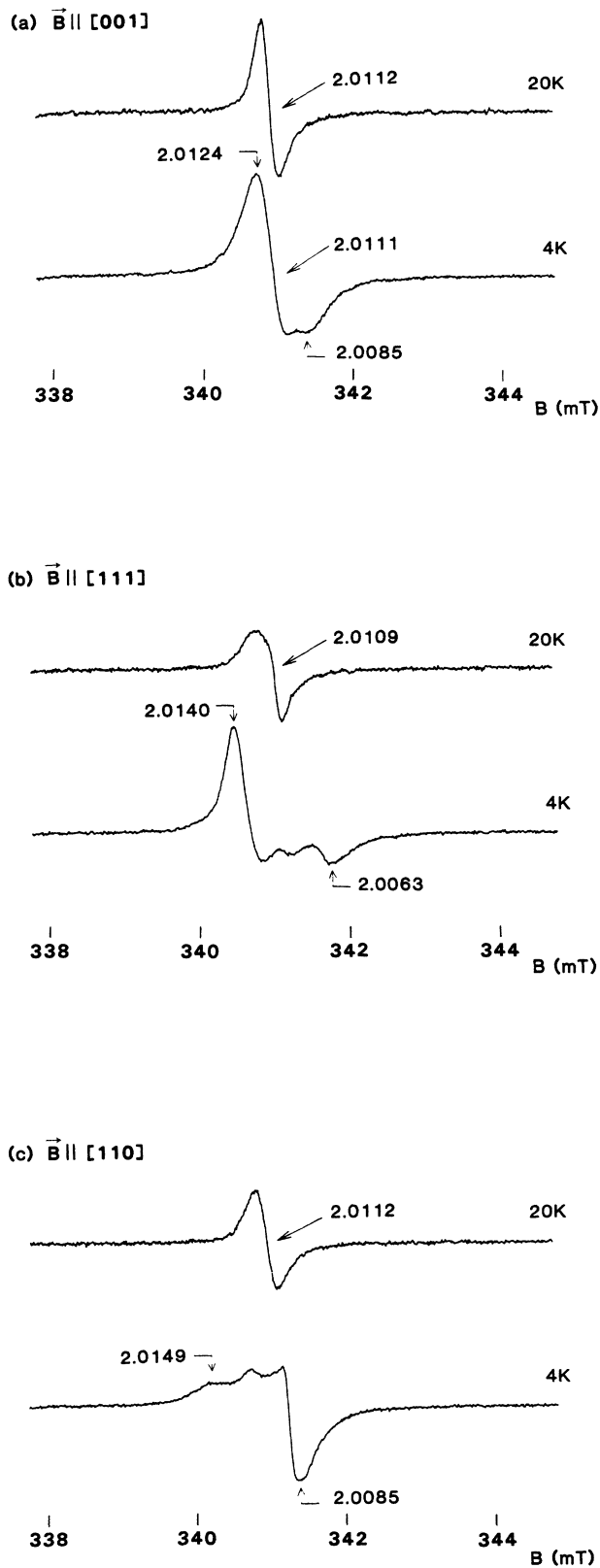
(a) $\vec{B} \parallel$ [001]

2.0112   20K

2.0124 ──┐

2.0111   4K

─ 2.0085

338   340   342   344   B (mT)

(b) $\vec{B} \parallel$ [111]

2.0109   20K

2.0140 ──┐

4K

─ 2.0063

338   340   342   344   B (mT)

(c) $\vec{B} \parallel$ [110]

2.0112   20K

2.0149 ──┐

4K

─ 2.0085

338   340   342   344   B (mT)

FIG. 3. cw EPR spectra of the NIRIM-1 center in synthetic diamond crystal E (ν=9.597 GHz, 100 kHz field modulation, 10 μW microwave power, 50 μT modulation amplitude) at 4 and 20 K.

state was confirmed by using a pulsed EPR technique.

The microwave pulse is characterized by the turning angle θ_p, through which the microwave magnetic field B_1 turns the electron spins: $\theta_p = \omega_n t_p$, where ω_n is the nutational frequency and t_p is the pulse width. If all $\Delta m_S = 1$ EPR transitions for the spin can be excited by the microwave pulse, then $\omega_n = \omega_1 = \gamma B_1$. If B_1 is sufficiently small that only a single transition in the spectrum is excited by the pulse (with the fine splitting larger than ω_1), ω_n depends on the matrix element of the $S_{\pm}$ operator for that transition.[15,16] The effective rotation for an $S=1$ spin is $2^{1/2}$ times that for an $S=\frac{1}{2}$ spin, if only one of the two transitions for an $S=1$ spin is excited. When only the $m_S = +\frac{1}{2}$ to $-\frac{1}{2}$ transition of a half-integral spin is excited, the effective rotation is $(S+\frac{1}{2})$ times that for an $S=\frac{1}{2}$ spin. In a two-pulse echo sequence (θ_{pI}-τ-θ_{pII}-τ-echo), with the interpulse delay τ fixed, the echo amplitude is proportional to $\sin\theta_{pI}\sin^2\frac{1}{2}\theta_{pII}$,[17] provided that the instantaneous spectral diffusion effect[18-20] is negligible. When the ratio between the turning angles is fixed to be $\theta_{pII}/\theta_{pI}=2$, $(\theta_{pI},\theta_{pII})$, which gives the maximum absolute value of the echo intensity, are (90°,180°), (270°,540°), and so on. The effective spin S can be determined if the echo intensity is measured as a function of the microwave pulse width t_p. The microwave pulse widths t_p were varied by varying the pulse width t_c of the control signal of the p-i-n diode switches ($t_p = t_c - a$, $a = \sim 25$ ns in our spectrometer).

In Ni$_s^-$, the $m_S = +\frac{1}{2}$ to $-\frac{1}{2}$ transition is predominantly observed at low temperatures, while the resonance frequencies of all three $\Delta m_S = 1$ transitions coincide to form a single line at high temperatures (~ 77 K). The $m_S = \pm\frac{3}{2}$ to $\pm\frac{1}{2}$ transitions are too broad to be observed at low temperatures, since the fine-structure splittings, which are presumably induced by symmetry lowering due to random internal strain or due to a distant charge compensating ion, have many different amplitudes and directions in the crystal. Thus, the spectrum appears to be a single line down to 4 K. We used sample F, which contains both Ni$_s^-$ and the NIRIM-1 center with the concentration sufficiently low enough for the instantaneous spectral diffusion effect to be negligible. Using the response from Ni$_s^-$ ($S=\frac{3}{2}$) to calibrate ω_1, the effective spin state for the anisotropic spectra at 4 K of the NIRIM-1 center was determined. The absolute value of the echo intensity was measured by varying the pulse widths t_{pI}, t_{pII} keeping the ratio $t_{pII}/t_{pI}\sim 2.0$. In this sample, Ni$_s^-$ exists predominantly in the distorted form at 40 K. For Ni$_s^-$, the extremal value of the absolute value of the echo intensity occurs with the interval of ~ 26 ns [Fig. 4(a)], which corresponds to $\omega_n/2\pi = 2\omega_1/2\pi = \sim 38$ MHz. The deviation from the sinosoidal form is ascribed to the presence of a nondistorted form that accounts for about 30% of the total signal. Keeping the microwave power (13 dB down from 1 kW), a similar measurement was carried out for the NIRIN-1 center at 4 K. From the interval ~ 48 ns ($\omega_n/2\pi = \sim 21$ MHz) of the extremal value of the absolute value of the echo intensity [Fig. 4(b)], the nutation frequency of the NIRIM-1 center is $\omega_n = \sim \omega_1$. The pulse width setting, which maximized the echo intensity of the
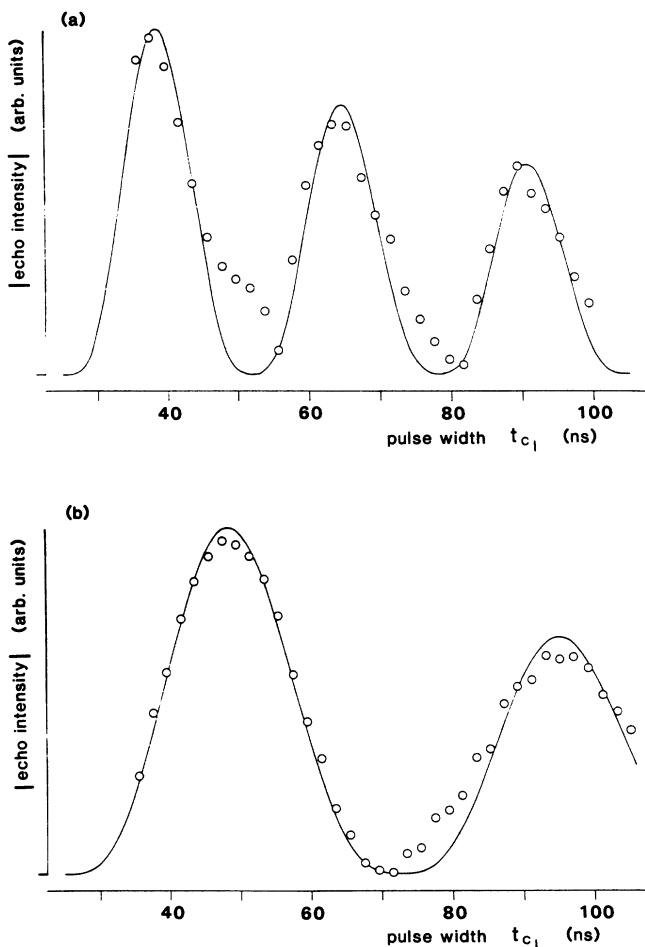
FIG. 4. Microwave pulse-width dependence of two-pulse echo intensity in synthetic diamond crystal F (microwave power 50 W, $\nu=9.3855$ GHz). (a) Distorted form of Ni_s^- ($S=\frac{3}{2}$) at 40 K with coexistence of a small fraction of undistorted form. (b) Distorted form of the NIRIM-1 center at 4 K. The absolute value of the echo intensity was measured by varying the widths of the control pulses of p-i-n diode switches (t_{cI}, t_{cII}) to be $(45.6+2k, 62.4+4k)$, and $k=0,1,2,\ldots$, (in ns). The spacing between the rising edges of the two control pulses was fixed to be 700 ns.

NIRIM-1 center, agrees with one usually used for a $S=\frac{1}{2}$ system in our spectrometer. Thus, the effective spin of the NIRIM-1 center is $S=\frac{1}{2}$.

B. NIRIM-2 center

In green-colored crystals (samples F and G) grown from Ni solvent with 2 wt. % Ti added, a new EPR spectrum, denoted NIRIM-2 here, was found by measuring at 4 K. Typical spectra are illustrated in Fig. 5. The angular dependence of the line positions is extremely large. For most orientations, the spectra (taken with a microwave power of 5 mW and detected in phase with 100 kHz field modulation) showed a line shape under a fast-
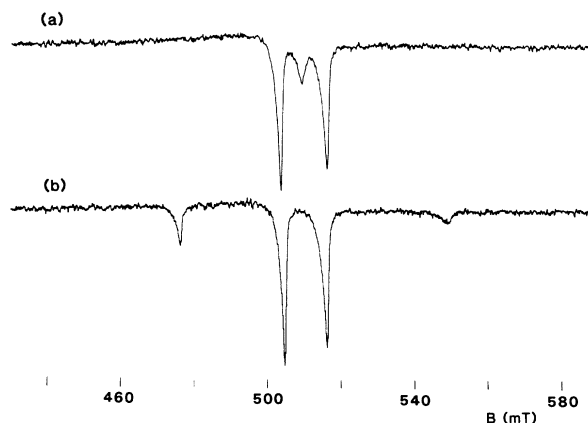

FIG. 5. cw EPR spectra of the NIRIM-2 center in synthetic diamond crystal F ($\nu=9.6017$ GHz, 100 kHz field modulation, 5 mW microwave power, 0.2 mT modulation amplitude) at 4 K. (a) the magnetic field parallel to near [001]. (b) rotated by 3° from the above orientation. The inequality in the signal intensity among the four sites seems to be caused by a preferential orientation (i.e., unequal population among the sites) in addition to the angular dependence of both the spin-lattice relaxation time and the transition probability.

passage condition.[21] For a few orientations where the signals appeared at $g>2$, the line shape was similar to an ordinary one. It is likely that the angular dependence of the spin-lattice relaxation time is large. The line positions for a rotation with the magnetic field perpendicular to the [$\bar{1}$10] axis are plotted in Fig. 6. The NIRIM-2 center consists of four sites. The rotation pattern as well as the number of sites indicates that the NIRIM-2 center has a trigonal symmetry. For trigonal centers in diamond, if four sites are equally populated, at most three lines of intensities 1:1:2 are expected for this rotation. Due to slight misalignment, a slight splitting between the two lines, which should always coincide with this rotation, was noticed. The angular dependence of the line positions is described, with the effective spin $\frac{1}{2}$, by a g tensor axially symmetric around a [111] axis with the principal values

$$g_{\parallel}=2.3285\pm0.0050, \quad g_{\perp}\approx0.0 . \tag{1}$$

The principal value $g_{\perp}$ could not be determined accurately, since the signals expected to appear at small g values were not observed due to a broad linewidth and/or the nonavailability of the corresponding magnetic-field strength at 9.6 GHz microwave frequency in our spectrometer. From the least-squares fitting of the line positions observed, by using the average of the two positions where the site splitting due to misalignment was noticed, we obtain $g_{\perp}=0.048$. However, the setting of $g_{\perp}=0$ reproduces the line positions observed well as shown in Fig. 6. When we discuss the electronic ground state by applying the crystal-field model to be described below, the assignment of the electronic ground state depends on whether $g_{\perp}=g_{\parallel}-g_e$ or $g_{\perp}=0$. The fitting with $g_{\perp}=g_{\parallel}-g_e$ was not as good as one with $g_{\perp}=0$. The concentration of the NIRIM-2 center for samples F and G is

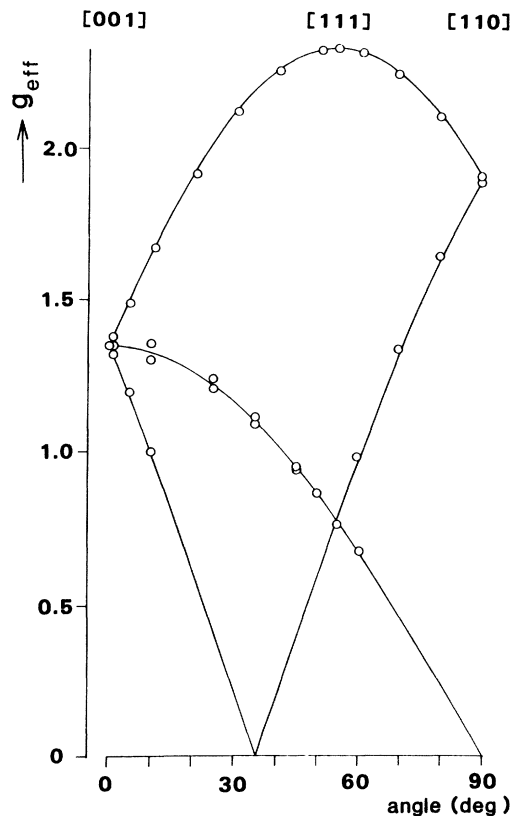FIG. 6. Angular dependence of the line position of the NIRIM-2 center as synthetic diamond crystal F rotated about the [$\bar{1}$10] axis at 4 K.
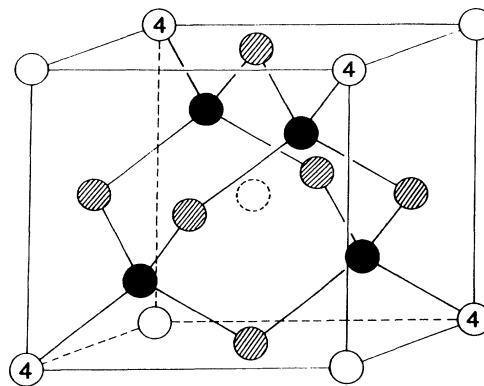

FIG. 7. Tetrahedral interstitial site of diamond surrounded by four nearest-neighbor carbon atoms and six next-nearest-neighbor carbon atoms. Third-nearest-neighbor carbon atoms, which are sited out of the cube indicated in the figure, are not included. Among the two sets of fourth-nearest-neighbor carbon atoms, those which are bonded to the nearest-neighbor carbons with C—C bond parallel to the [111] axis are labeled 4.

estimated to be 1 ppm and 0.8 ppm, respectively, from the EPR signal intensities.

IV. DISCUSSION

A. NIRIM-1 center

1. Site and charge state

Observation of the isotropic spectrum above $\sim$25 K suggests that the Ni giving the NIRIM-1 spectrum occupies a high-symmetry site and that no other impurities or vacancies are locally associated. In diamond, there are two tetrahedral sites: a substitutional site and an interstitial site. Both sites are surrounded tetrahedrally by four nearest-neighbor carbons 1.54 Å apart. The substitutional site has twelve next-nearest neighbors 2.52 Å apart, while the interstitial site has six next-nearest neighbors 1.78 Å apart (Fig. 7). Although a definitive assignment of the site should be given based on the ^{13}C superhyperfine couplings of surrounding carbons, the determination of the effective spin is sufficient to discuss the site and the charge state if an appropriate theoretical model is available.

Theoretical studies on the electronic structure of transition-metal impurities in silicon has progressed remarkably in the last decade.[22-24] However, transition-

metal impurities in diamond have not attracted extensive theoretical studies, yet. Here we will discuss the site and the charge state of the Ni giving the NIRIM-1 spectrum by applying two simple models: the Ludwig-Woodbury model[25,26] and the vacancy model of Watkins.[27]

a. Ludwig-Woodbury model. The model of Ludwig and Woodbury has been successfully applied for describing qualitatively the electronic structure of transition-metal impurities that form deep states in silicon and in many other semiconductors. In the substitutional site of silicon, transition-metal ions having a free-ion configuration $3d^n4s^2$ are expected to have an electronic configuration $3d^{n-2}$, since four $3d$ electrons are transferred to the valence shell to complete the tetrahedral bondings to their four nearest neighbors. The tetrahedral crystal field from the nearest neighbors splits the $3d$ orbitals into the subsets e and t_2, with the e lower in energy. In the interstitial site of silicon, transition-metal ions having a free-ion configuration $3d^n4s^2$ are expected to have an electronic configuration $3d^{n+2}$, since the $4s$ electrons are transferred to the $3d$ shell. The $3d$ orbitals are split into the subsets t_2 and e, with t_2 lower in energy. It is likely that the octaheral field from the next-nearest neighbors dominates over the tetrahedral field from the nearest neighbors. In both cases, the e and t_2 states associated with the metal d orbitals are located within the energy gap and are filled in such a way that the maximum spin S is attained (Hund's rule).

By applying the Ludwig-Woodbury model, the electronic configurations and the spin multiplicities of nickels that might occur in diamond are illustrated in Fig. 8. Here, highly charged states Ni^{n+},Ni^{n-} ($n \geq 2$) are excluded. With the effective spin $S = \frac{1}{2}$, the NIRIM-1 spectrum is assignable to interstitial Ni^+, denoted Ni_i^+, with the electronic configuration $3d^9$ ($t_2^6e^3$). The EPR spectrum of Ni_i^+ in silicon has been reported.[26] Assignment of the effective spin $S = \frac{1}{2}$ was confirmed by observation of an anisotropic spectrum ($g_1 = 2.0133$, $g_2 = 2.0357$,
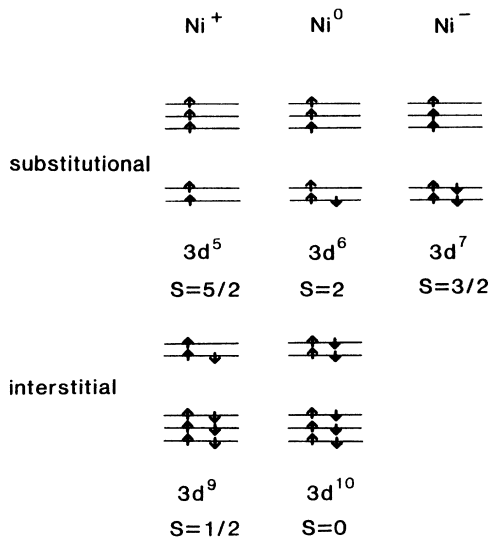
FIG. 8. Electronic configuration and spin multiplicity of Ni centers in diamond.

$g_3 = 2.0333$ with the principal directions along [111], [110], and [112], respectively) consisting of several geometrically nonequivalent sites below ~ 2 K. The spectrum is isotropic ($g = 2.026$) between 10 and 20 K due to rapid reorientation.

According to the Ludwig-Woodbury model, Ni_i^+ in diamond has an orbitally degenerate ground state ^2E, which should exhibit EPR spectra with those features characteristic of the Jahn-Teller effect. Transition-metal ions with a ^2E ground state in cubic symmetry have provided some classical examples of EPR investigations of the Jahn-Teller effect.[28] Their low-temperature EPR spectra may be classified into three types: static, dynamic, and intermediate Jahn-Teller effects.[29-31] The two-fold degenerate state ^2E couples with the E mode of vibrations, i.e., tetragonal distortion modes. A static Jahn-Teller effect is characterized by the presence of three magnetically inequivalent sites at low temperature. The line positions are given by

$$B = (h\nu/\mu_B)(g_\parallel^2\cos^2\theta + g_\perp^2\sin^2\theta)^{-1/2} , \quad (2)$$

where θ is the angle of the magnetic field with respect to one of three cubic fourfold axes along which the tetragonal distortion occurs. The associated line shape is symmetrical having the usual Gaussian or Lorentzian shapes. Three superimposed axially symmetric spectra will be motionally averaged through thermally induced reorientation among the three equivalent static distortions, and a resultant isotropic spectrum will be observed.

For the dynamic Jahn-Teller effect, a single strain-broadened EPR line is present at low temperature. The line has a roughly symmetrical powderlike shape dominated by two extremes. The line positions of the two extremes are given to the first order by

$$B_\pm = (h\nu/g_1\mu_B)$$

$$\times \{1 \pm qg_2/g_1[1 - 3(m^2n^2 + n^2l^2 + l^2m^2)]^{1/2}\} , \quad (3)$$

where g_1 and qg_2 are the two parameters required for the Zeeman interaction ($g_1 \gg qg_2$) and l,m,n are the direction cosines of the magnetic field with respect to the cubic fourfold axes. For $\mathbf{B}\|[100]$, the two extremes have their largest separation. For $\mathbf{B}\|[111]$, this separation is essentially zero, giving a line with a more conventional line shape at $g = g_1$. The intensity of this powderlike spectrum decreases with increasing temperature until it is replaced by an isotropic line at $g = g_1$ that appears superimposed with the powderlike spectrum. The isotropic line can result from the averaging of part of the powder-like spectrum by rapid vibronic relaxation, by thermal population of the nearest excited vibronic singlet level, or by a combination of these two.

For the intermediate Jahn-Teller effect, the features of the dynamic Jahn-Teller effect are modified: (i) a selective broadening and shifting of one extreme, (ii) a departure of the angular variation of the spectrum from that associated with a pure dynamic or pure static Jahn-Teller effect, and (iii) the presence of an unusually complex line shape for orientations corresponding to $\mathbf{B}\|[111]$.

The isotropic spectra at high temperatures and the anisotropic spectra at low temperatures suggest that the NIRIM-1 spectrum arises from a Jahn-Teller system. The features of NIRIM-1 at low temperatures seem to fit those of the intermediate Jahn-Teller effect except that the angular variation indicates that a trigonal distortion, rather than a tetragonal distortion, is predominantly involved. It is only those lattice distortions that belong to the irreducible representation E of the group O or T_d that can cause a first-order splitting of a doublet ^2E state and thus lead to a Jahn-Teller coupling as long as spin-orbit coupling is ignored. Thus, the ^2E state undergoes a tetragonal distortion in normal cases. Here, we need some mechanism that does bring a trigonal distortion to our case with a ground state ^2E. The spin-orbit interaction, while not splitting a ^2E state, might mix the ground state ^2E with the excited orbital triplet state, which can couple with both tetragonal (E) and trigonal (T_2) modes. At the interstitial site, the energy splittings of $3d$ electrons are determined by the octahedral field from the second-nearest-neighbor carbons. Since the e electrons do not form σ bonding with the nearest neighbors, the coupling of the ^2E state with the E mode of nuclear motion might be weak. Trigonal distortions arising from the higher-order effect might dominate over the tetragonal distortions. There are some examples that indicate that a trigonal Jahn-Teller effect might possibly occur, if a trigonal strain were strong and if the coupling to the tetragonal vibrations were weak. In Ni^+:GaP and Ni^+:GaAs, the ^2E excited state of the electronic configuration $3d^9$ under the tetrahedral field was studied by the uniaxial stress experiments of the zero-phonon line of the $^2T_2 \rightarrow {}^2E$ transition. The large sensitivity to trigonal stress observed is ascribed to an unusual coupling of the ^2E excited state to trigonal vibrations.[32] In Y^{2+}:SrCl$_2$, the EPR spectra under uniaxial stress revealed that the ^2E ground state of the electronic configuration $4d^1$ under the cubic crystal field has strong coupling to trigonal vibrations.[33]

b. Vacancy model. From the Ludwig-Woodbury mod-

el, the electronic ground state of Ni_s^-, both in silicon and in diamond, is an orbitally nondegenerate $^4A_2$ state (electronic configuration $e^4t_2^3$) having the effective spin $S = \frac{3}{2}$. In fact, Ni_s^- in silicon shows an $S = \frac{3}{2}$ spectrum with the principal axes [$\bar{1}10$], [110], and [001].[34] In the "vacancy" model, Ni_s^- is considered as a neutral Ni atom (Ni^0) with a closed shell ($3d^{10}$) sitting in a negatively charged vacancy V^-. With an on-center Ni ion of a filled $3d^{10}$ shell, three electrons occupy orbitals of t_2 symmetry located primarily on the four nearest silicon neighbors. The degeneracy of the partly filled t_2 orbitals is lifted by a static Jahn-Teller distortion resulting in a [001] orientation of the defect and the effective spin $S = \frac{1}{2}$.

From the vacancy model, substitutional transition-metal impurities in the charge states M^+, M^0, M^- are expected to have structure resulting from symmetry-lowering Jahn-Teller distortions similar to that of corresponding charge states V^+, V^0, V^- of single vacancy. The electronic structure of the vacancy is described by using the one-electron molecular-orbital treatment. In a nondistorted structure of T_d symmetry, the linear combination of the four broken bonds on the atoms around the vacancy forms the defect molecular orbitals: an a_1 singlet and a t_2 triplet, with a_1 lower in energy. The positively charged vacancy V^+ has three electrons. A $^2T_2$ state (electronic configuration $a_1^2t_2$) is unstable against tetragonal or trigonal distortion. In the case of V^+ in silicon, tetragonal Jahn-Teller distortion has lowered the symmetry to D_{2d}. In the case of V^- in silicon, tetragonal Jahn-Teller distortion with additional trigonal Jahn-Teller distortion has lowered the symmetry to C_{2v} resulting in the effective spin $S = \frac{1}{2}$. That the Jahn-Teller splitting of ^2E, the lowest doublet of t_2^3, is sufficient to bring one component down below $^4A_2$ is a rather extraordinary case.

In diamond, the ground state of the negatively charged vacancy V^- is likely to be an orbitally nondegenerate $^4A_2$ (electronic configuration $a_1^2t_2^3, S = \frac{3}{2}$) that is not subject to Jahn-Teller distortion. It has been suggested that the ND1 optical-absorption band, an electric dipole transition between an orbitally nondegenerate ground state and a triply degenerate excited state at a tetrahedral defect, is associated with a negatively charged vacancy.[35] The ND1 band is strongest in irradiated type-Ib diamond that contains single substitutional nitrogen atoms as major impurities.[36] We note that the effective spin $S = \frac{3}{2}$ and the absence of the Jahn-Teller distortion of Ni_s^- in diamond is explainable both by using the Ludwig-Woodbury model and by using the vacancy model.

If the vacancy model is applicable to Ni centers in diamond, the NIRIM-1 spectrum having the effective spin $S = \frac{1}{2}$ is assignable to substitutional Ni^+, denoted Ni_s^+. Since the electronic ground state $^2T_2$ of the positively charged vacancy V^+ in T_d symmetry is unstable against tetragonal and/or trigonal distortions, the trigonal distortion of the NIRIM-1 center at 4 K is explainable as a first-order Jahn-Teller distortion by the vacancy model. The vacancy model predicts that the wave function of the unpaired electron(s) should be mostly dangling bond like. The EPR spectrum labeled S1 ($S = \frac{1}{2}$) in electron-

irradiated type-IIa diamond crystal was ascribed to either positively charged vacancy V^+ or negatively charged vacancy V^-.[37] The ^{13}C superhyperfine interactions from the four nearest-neighbor carbons ($A_\parallel/g\beta = 5.0480$ mT, $A_\perp/g\beta = 2.9180$ mT) and from the twelve next-nearest neighbor carbons ($A_\parallel/g\beta = 0.4750$ mT, $A_\perp/g\beta = 0.3320$ mT) were observed. In the NIRIM-1 spectrum, since the ^{13}C superhyperfine structure was not resolved from the strong main line, the ^{13}C superhyperfine splitting is expected to be considerably smaller than that of S1. In samples C, E, F, and G, Ni_s^- coexists with the NIRIM-1 center. Unless the electronic levels in the gap of Ni_s^- and Ni_s^+ are close, these two different charge states are not likely to coexist. Unless strong Jahn-Teller stabilization lowers the electronic level of Ni_s^-, the electronic positions in the gaps are well separated between these two. Thus, we are inclined to take the Ludwig-Woodbury model for the NIRIM-1 center.

2. Charge compensation

Based on the above discussion, we assume that the NIRIM-1 spectrum is arising from Ni_i^+. Transition-metal ions in silicon, both substitutional and interstitial, can occur in various charge states. The desired charged state is obtainable by adjusting the Fermi-level position with the proper concentration of shallow donors or shallow acceptors. It seems that similar control of the charge state is applicable for nickel atoms in diamond. In the boron-doped semiconducting crystal (samples K, M, and N), a strong Ni_i^+ spectrum was observed, while no Ni_s^- resonance was detected. Our assignment of the positive charge to the NIRIM-1 center is confirmed by the observation of the increase of its concentration in p-type semiconducting diamonds. The increase of the conductivity by boron doping is efficiently achieved by co-using nitrogen getters (Table I). When nitrogen getters are not added, it is likely that the boron atoms incorporated are first used for compensating the nitrogen atoms. In the heavily boron-doped crystals (samples L and O), EPR signals of Ni_i^+ were not observed. It is probable that, at high doping levels, nickel atoms might be incorporated as impurity-acceptor pairs.

In the insulating crystals, samples C, E, F, and G, grown from the Ni solvent with the nitrogen getters added, Ni_s^- and Ni_i^+ coexist. Although the charge states are different, the electric level positions of Ni_s^-, Ni_i^+ in the energy gap are likely to be close so that the two levels can be simultaneously occupied if the Fermi-level position is suited. Since these crystals exhibit nonuniform color distribution, these two centers might be segregated in different sections of the crystals. In these crystals, the concentration of Ni_i^+ is not matched with that of Ni_s^-. Although these two centers are, partly, charge compensating each other, some other charged defects are needed to maintain charge neutrality of the lattice. Since the EPR spectrum of Ni_i^+ shows high symmetry above ~ 25 K, the charge-compensating ions (defects) are located a large distance apart.

From EPR measurements, we cannot conclude whether some of our crystals contain Ni impurities in a neutral

charge state or not. Interstitial Ni^0 (Ni_i^0) of the closed shell ($3d^{10}$) does not give EPR signals. Substitutional Ni^0 (Ni_s^0) having the electronic configuration $3d^6$ is not easily observable by EPR, since the ground state $^5E(e^3t^3)$ has an integral spin $S=2$. At present, it is difficult to decide whether the growth-condition dependence of the concentration $[Ni_i^+]$ ($[Ni_s^-]$) is accompanied by the variation of the total concentration of interstitial (substitutional) nickel impurities, or whether it is caused by variation in the distribution among the different charge states of interstitial (substitutional) nickel impurities.

B. NIRIM-2 center

The free-ion ^2D term of $3d^1$ or $3d^9$ electronic configuration is split into ^2E and $^2T_2$ under a tetrahedral or octahedral crystal field. The orbitally degenerate ^2E state is not split in first order just by a trigonal distortion or just by spin-orbit coupling. With a combination of trigonal distortion and spin-orbit coupling, the ^2E state is split in second order into two Kramers doublets, Γ_6 and $\Gamma_4\Gamma_5$. The principal values of the g tensor for these states are for Γ_6,

$$g_\parallel = 2 - \frac{4k'\zeta'}{\Delta}, \quad g_\perp = \frac{4k'\zeta'}{\Delta}, \tag{4}$$

and for $\Gamma_4\Gamma_5$

$$g_\parallel = 2 - \frac{4k'\zeta'}{\Delta} + \frac{8k'K'}{\Delta}, \quad g_\perp = 0, \tag{5}$$

where Δ, ζ', k', K' are the cubic crystal-field splitting, the spin-orbit coupling between the ^2E and $^2T_2$, and the parameters to take into account the covalency effects.[38] The above g values were originally obtained for the excited states of $3d^9$ electronic configuration in a crystal field of trigonally distorted tetrahedron to interprete the Zeeman splitting of the optical spectra of Cu^{2+} in hexagonal ZnO.[39,40] These equations are applicable to the ground state of either $3d^1$ in trigonally distorted tetrahedron or $3d^9$ in trigonally distorted octahedron by taking proper signs. Since $\Delta \gg k'\zeta', k'K'$, we note that $g_\parallel \approx 2$ and $g_\perp \approx 0$ for both Γ_6 and $\Gamma_4\Gamma_5$. As described above, the line positions observed fit much better with $g_\perp = 0$ than with $g_\perp = g_\parallel - g_e$; therefore, the ground state of the NIRIM-2 center is $\Gamma_4\Gamma_5$. Thus, the NIRIM-2 center is related to transition-metal impurities. The crystals that gave the NIRIM-2 spectra were grown from the Ni solvent with the addition of a small amount of Ti. Substitutional Ti^- is expected to show an electronic configuration $3d^1$. However, since the g shift for the ground state is less than zero for a paramagnetic ion whose unfilled shell is less than half full, substitutional Ti^- with an additional trigonal distortion is not likely the case for the NIRIM-2 center. From the composition of the metal solvent used, it is likely that the NIRIM-2 center is arising from a Ni center with electronic configuration $3d^9$ in a crystal field of trigonally distorted octahedron. In the interstitial sites, although the nearest neighbors are four carbons in tetrahedral arrangement, the crystal-field splitting of $3d$ electrons is predominatly determined by six next-

nearest-neighbor carbons in octahedral arrangement. A trigonal distortion might be achieved by distortion of the octahedron of the next-nearest neighbors and/or by distortion of the tetrahedron of the nearest neighbors. Since the NIRIM-1 center has been assigned to an isolated Ni^+ ($3d^9$) at the interstitial site, the NIRIM-2 center is accompanied by a nonparamagnetic vacancy or by some nearby nonparamagnetic impurity. The trigonal field might be produced either by vacancy association or by local charge compensation. The EPR signal of NIRIM-2 did not show any hyperfine structure due to nearby impurity atoms having nuclear spin. Thus, perhaps one of the four nearest-neighbor carbons or one of the eight fourth-nearest-neighbor carbons might be missing as neutral vacancy V^0.

V. CONCLUSION

Two new EPR spectra labeled NIRIM-1 and NIRIM-2, respectively, in synthetic diamond crystals are assigned to be associated with interstitial Ni^+ with the electronic configuration $3d^9$. Incorporation of nickel impurities is controllable by varying the composition of metal solvent and/or by varying the doping level of borons. So far, transition-metal impurities incorporated in a dispersed form in synthetic diamond crystals seem to be limited to Ni. The EPR spectra suggested to be arising from other transition-metal impurities were reported; however, the assignments have not been established yet.[41,42] It should be noted that, to obtain the crystals for which strong signals of Ni_i^+ are observable, either the amount of the nitrogen getters or the amount of boron atoms added to the Ni solvent needs to be carefully chosen. Thus, in searching for a new transition-metal impurity by varying the growth conditions, selection of the composition of the metal solvent and the doping level of boron might be crucial.

The NIRIM-1 center is likely to be an isolated interstitial Ni^+, denoted Ni_i^+, with the orbitally degenerate ground state ^2E. It is plausible that the anisotropic powderlike spectra at 4 K is due to an intermediate Jahn-Teller effect coupled, predominantly, to trigonal distortions (strains). The distorted configuration of Ni_i^+ in silicon below 2 K might be ascribed to a static Jahn-Teller effect. The g tensor is nearly axial symmetric with the unique axis parallel to [111]. It is likely that a trigonal distortion is predominantly involved. The principal value along [111] is smaller than the other two principal values. In the anisotropic powderlike spectra of Ni_i^+ in diamond at 4 K, the g value corresponding to the high-field extreme takes the smallest value at the magnetic field parallel to [111]. Thus, the anisotropy of the g tensor of Ni_i^+ in diamond seems to be similar to that of Ni_i^+ in silicon.

By comparing the structure of neutral vacancy V^0 between silicon and diamond, it was pointed out that there is a higher resistance against moving the neighboring atoms in a tetragonal motion at the vacancy of diamond than at the vacancy of silicon.[43] As is evident in the example of the isolated substitutional nitrogen atoms,[44] a relatively large displacement is allowed along the C—C

bond direction. In diamond, such a distortion that involves a bending of the bond might be less likely to occur than one that involves a radial movement of atoms. In the case of Ni_i^+, the distortion is likely to be predominantly trigonal, both in silicon and in diamond. When impurities are incorporated, lattice distortion such as elongation of the interatomic distances should be required to attain the energy minimum configuration. Comparison of the extent of the lattice distortions allowed (the strength of Jahn-Teller coupling) and the strength and the distribution of the random internal strains, with respect to the same impurity ion, between silicon and diamond, will be helpful in understanding the electron-lattice interaction in diamond of an extreme co-

valent form of crystal bonding.

The NIRIM-2 center arises from interstitial Ni^+ (electronic configuration $3d^9$) in a crystal field of a trigonally distorted octahedron. The trigonal field is likely to be caused by vacancy association or by local charge compensation.

Recently, the optical center of a 1.40-eV system was identified to be a Ni center having trigonal symmetry with a doubly degenerate orbital ground state ($S = \frac{1}{2}$) split by spin-orbit interaction.[45] Thus, the 1.40-eV optical center is closely related to our new EPR centers. Further studies are needed to determine whether one of two new EPR spectra are arising from the optical 1.40-eV center or not.

[1] J. H. N. Loubser and W. P. van Ryneveld, Nature 211, 517 (1966).

[2] M. I. Samoilovich, G. N. Bezrukov, and V. P. Butuzov, Pis'ma Zh. Eksp. Teor. Fiz. 14, 551 (1971) [JETP Lett. 14, 379 (1971)].

[3] J. Isoya, H. Kanda, J. R. Norris, J. Tang, and M. K. Bowman, Phys. Rev. B 41, 3905 (1990).

[4] A. T. Collins and P. M. Spear, J. Phys. D 15, L183 (1982).

[5] A. T. Collins and P. M. Spear, J. Phys. C 16, 963 (1983).

[6] A. T. Collins, J. Phys. Condens. Matter 1, 439 (1989).

[7] G. Davies, A. J. Neves, and M. H. Nazaré, Europhys. Lett. 9, 47 (1989).

[8] R. H. Wentorf, Jr., J. Phys. Chem. 75, 1833 (1971).

[9] H. M. Strong and R. M. Chrenko, J. Phys. Chem. 75, 1838 (1971).

[10] H. M. Strong and R. E. Tuft, U.S. Patent No. 4034066 (1977).

[11] H. M. Strong, U.S. Patent No. 4082185 (1978).

[12] The EPR spectrum of the paramagnetic center in diamond has been conventionally labeled by using the initial letters of the research group that first reported it and by using a serial number within the group. We use, here, "NIRIM" instead of "NI", since the latter might cause confusion by implying that the center is associated with Ni.

[13] R. M. Chrenko, Phys. Rev. B 7, 4560 (1973).

[14] F. S. Ham, G. W. Ludwig, G. D. Watkins, and H. H. Woodbury, Phys. Rev. Lett. 5, 468 (1960).

[15] F. M. M. Geurts, A. P. M. Kentgens, and W. S. Veeman, Chem. Phys. Lett. 120, 206 (1985).

[16] A. P. M. Kentgens, J. J. M. Lemmens, F. M. M. Geurtz, and W. S. Veeman, J. Magn. Reson. 71, 62 (1987).

[17] W. B. Mims, in Electron Paramagnetic Resonance, edited by S. Geschwind (Plenum, New York, 1972), pp. 263–351.

[18] J. R. Klauder and P. W. Anderson, Phys. Rev. 125, 912 (1962).

[19] I. M. Brown, in Time Domain Electron Spin Resonance, edited by L. Kevan and R. N. Schwartz (Wiley, New York, 1979), pp. 195–229.

[20] K. M. Salikhov and Yu. D. Tsvetkov, in Time Domain Electron Spin Resonance, edited by L. Kevan and R. N. Schwartz (Wiley, New York, 1979), pp. 231–277.

[21] M. Weger, Bell Syst. Tech. J. 39, 1013 (1960).

[22] U. Lindefelt and A. Zunger, Phys. Rev. B 30, 1102 (1984).

[23] A. Fazzio, M. J. Caldas, and A. Zunger, Phys. Rev. B 32, 934 (1985).

[24] A. Zunger, in Solid State Physics, edited by H. Ehrenreich and

D. Turnbull (Academic, New York, 1986), Vol. 39, pp. 275–464.

[25] G. W. Ludwig and H. H. Woodbury, Phys. Rev. Lett. 5, 98 (1960).

[26] G. W. Ludwig and H. H. Woodbury, in Solid State Physics, edited by F. Seitz and D. Turnbull (Academic, New York, 1962), Vol. 13, pp. 223–304.

[27] G. D. Watkins, Physica 117B&118B, 9 (1983).

[28] F. S. Ham, in Electron Paramagnetic Resonance, edited by S. Geschwind (Plenum, New York, 1972), pp. 1–119.

[29] R. W. Reynold, L. A. Boatner, M. M. Abraham, and Y. Chen, Phys. Rev. B 10, 3802 (1974).

[30] R. W. Reynolds and L. A. Boatner, Phys. Rev. B 12, 4735 (1975).

[31] H. Bill, in The Dynamical Jahn-Teller Effect in Localized Systems, edited by Yu. E. Perlin and M. Wagner (North-Holland, Amsterdam, 1984), pp. 709–817.

[32] B. Clerjaud, J. Phys. C 18, 3615 (1985).

[33] H. Bill and D. Lovy, J. Phys. Condens. Matter 1, 10265 (1989).

[34] L. S. Vlasenko, N. T. Són, A. B. van Oosten, C. A. J. Ammerlaan, A. A. Lebedev, E. S. Taptygov, and V. A. Khramtsov, Solid State Commun. 73, 393 (1990).

[35] G. Davies and E. C. Lightowlers, J. Phys. C 3, 638 (1970).

[36] G. Davies, Nature 269, 498 (1977).

[37] J. A. Baldwin, Jr., Phys. Rev. Lett. 10, 220 (1963).

[38] U. Scherz, J. Phys. Chem. Solids 30, 2077 (1969).

[39] R. E. Dietz, H. Kamimura, M. D. Sturge, and A. Yariv, Phys. Rev. 132, 1559 (1963).

[40] I. Broser, U. Scherz, and M. Wöhlecke, J. Lumin. 1-2, 51 (1970).

[41] V. S. Bagdasaryan, E. A. Markosyan, M. A. Matosyan, O. S. Torosyan, and E. G. Sharoyan, Fiz. Tverd. Tela (Leningrad) 17, 1518 (1975) [Sov. Phys. Solid State 17, 991 (1975)].

[42] J. H. N. Loubser and J. A. van Wijk, South Afr. J. Phys. 10, 165 (1987).

[43] G. Davies, Rep. Prog. Phys. 44, 787 (1981).

[44] W. V. Smith, P. P. Solokin, I. L. Gelles, and G. J. Lasher, Phys. Rev. 115, 1546 (1959).

[45] M. H. Nazaré, A. J. Neves, and G. Davies, in Diamond, Boron Nitride, Silicon Carbide and Related Wide Bandgap Semiconductors, Proceedings of the MRS Fall Meeting, Boston, Massachusetts, 1989, Vol. 162 of MRS Popular Series, edited by J. T. Glass, R. F. Messier, and N. Fujimori (Materials Research Society, Pittsburgh, in press).